Hindawi
Journal of Nanotechnology
Volume 2018, Article ID 4657040, 10 pages
https://doi.org/10.1155/2018/4657040

*Research Article*

# Bifunctional Tailoring of Platinum Surfaces with Earth Abundant Iron Oxide Nanowires for Boosted Formic Acid Electro-Oxidation

**Bilquis Ali Al-Qodami,[1] Heba H. Farrag,[1,2] Sayed Youssef Sayed,[1] Nageh K. Allam,[2] Bahgat E. El-Anadouli,[1] and Ahmad M. Mohammad[1]**

[1]*Chemistry Department, Faculty of Science, Cairo University, Cairo 12613, Egypt*
[2]*Energy Materials Laboratory, School of Sciences and Engineering, The American University in Cairo, New Cairo 11835, Egypt*

Correspondence should be addressed to Ahmad M. Mohammad; ammohammad@cu.edu.eg

Received 30 August 2018; Revised 13 October 2018; Accepted 11 November 2018; Published 3 December 2018

Guest Editor: Kunal Mondal



To expedite the marketing of direct formic acid fuel cells, a peerless inexpensive binary FeOx/Pt nanocatalyst was proposed for formic acid electro-oxidation (FAO). The roles of both catalytic ingredients (FeOx and Pt) were inspired by testing the catalytic performance of FAO at the FeOx/Au and FeOx/GC analogies. The deposition of FeOx proceeded electrochemically with a post-activating step that identified the catalyst's structure and performance. With a proper adaptation for the deposition and activation processes, the FeOx/Pt nanocatalyst succeeded to mitigate the typical CO poisoning that represents the principal element deteriorating the catalytic performance of the direct formic acid fuel cells. It also provided a higher (eightfold) catalytic efficiency than the bare Pt substrates toward FAO with a much better durability. Field-emission scanning electron microscopy (FE-SEM), energy-dispersive X-ray spectroscopy (EDX), and X-ray diffraction (XRD) were all employed to inspect, respectively, the surface morphology, bulk composition, and crystal structure of the catalyst. The electrochemical impedance spectra could correlate the charge transfer resistances for FAO over the inspected set of catalysts to explore the role of FeOx in mediating the reaction mechanism.

## 1. Introduction

The global desire to sustain new green paths toward a low carbon future has motivated research and development in the industry of fuel cells (FCs) and hydrogen production. In 2016, the expansion and inroads of these industries surpassed expectations to realize additional uses in ground support equipment, drayage and long-haul trucks, passenger trains, delivery vans, carbon capture from natural gas-fired power generation and oil sands sites, and energy storage [1]. Basically, FCs are galvanic reactors combining a fuel continuously with oxygen to produce electricity, water, and heat. Unlike combustion technologies, FCs do not burn fuel, making the process quiet, pollution-free, and up to 2-3 times more efficient [1, 2]. The $H_2/O_2$ FCs (HFCs) received for long time the eminent effort since the invention by Sir William Robert Grove in 1839 passing by its real production by General Electric Company (1950) and utilization in Gemini space mission (1962) [3–5]. Right now, the HFCs operate a wide range of potential applications in transportation and in stationary and portable power services. Although satisfying the highest cleaning criteria particularly when $H_2$ is provided from renewable non-polluting sources, the HFCs failed to meet the safety standards related to the production, usage, transporting, and storing of the $H_2$ fuel which is highly flammable. This, in addition to the low energy density of $H_2$ and the high cost of miniaturization of gaseous $H_2$ containers, encouraged the movement into realizing liquid FCs (LFCs). In this regard, different alcohols (methanol, ethanol, propanol, and ethylene glycol) and non-alcohols (formic acid, dimethyl ether, hydrazine, ammonia, borane, and sodium borohydride) were recommended as replacements for the $H_2$ fuel [6–8]. Nevertheless, formic acid (FA) which is inflammable and non-toxic (typically known

as a food-additive) has shown a particular interest for the FCs' technology [9]. Indeed, the direct formic acid FCs (DFAFCs) that operate with the FA electro-oxidation (FAO) [10–14] enjoys several merits including the relatively low operating temperature, high practical power density, small crossover flux through Nafion membranes, rapid electro-oxidation kinetics making them highly efficient, and high open circuit voltage (1.45 V) [15–18]. Yet, the commercialization of DFAFCs is encountered by the critical poisoning of the Pt catalyst (dedicated for FAO) with CO released with the non-faradaic dissociation of FA even at open circuit potential. This poisoning inducts a catalytic impairment for Pt to support FAO directly at low potential which ultimately deteriorates the performance of DFAFCs [6, 19–24]. In order to prepare the DFAFCs for a proper competition with HFCs, the CO poisoning of the anodic Pt substrates has to be overcome. The essence of this overcoming lies in modulating the Pt-CO binding to mitigate the adsorption of CO on the Pt surface and enriching the Pt surface with oxygen containing moieties that facilitates the oxidative removal of poisoning CO at a relatively low potential. Interestingly, the use of hybrid nanocatalysts of Pt with Pd, Au, Ru, Rh, Bi, Sn, Co, Cu, and Ni or with transition metal oxides such as NiOx, CoOx, MnOx, and $Cu_2O$ for FAO succeeded to provide a proof for this conception [24–30]. The current investigation suggests a low-priced and efficient FeOx/Pt nanocatalyst for FAO. The modification of bare Pt electrodes with FeOx is intended to utilize a cheap (earth-abundant) modifier (Fe species) to boost the catalytic activity of conventional Pt anodes toward FAO. Generally, the utilization of transition metal and/or transition metal oxides is sought to mediate the mechanism of FAO to facilitate the charge transfer and ultimately improve the reaction kinetics. Interestingly, with a proper activation, a reasonable mitigation for CO poisoning was afforded while sustaining an improved catalytic performance toward FAO.

## 2. Experimental

*2.1. Materials and Pretreatment.* All chemicals utilized in this investigation were of analytical grades and used without prior treatments. Doubled distilled water was used to rinse the electrodes and to prepare the involved aqueous solutions. Iron (II) sulfate heptahydrate ($FeSO_4.7H_2O$) and sodium hydroxide pellets were purchased from Riedel-de Haen and Sigma-Aldrich, respectively. Polycrystalline platinum (Pt: $d$ = 3.0 mm), gold (Au: $d$ = 3.0 mm), and glassy carbon (GC: $d$ = 6.0 mm) electrodes served as the working electrodes, while an Ag/AgCl/KCl (sat.) and a Pt spiral wire were used as reference and counter electrodes, respectively. All potentials will next be read in reference to the Ag/AgCl/KCl (sat.) electrode. Conventional cleaning treatments were applied to clean the Pt, Au, and GC electrodes which were mechanically polished with aqueous slurries of fine alumina powder and then sonicated and washed with doubly distilled water [31]. Moreover, the Pt electrode was electrochemically pretreated in 0.5 M $H_2SO_4$ solution by cyclic potential between −0.2 and 1.3 V at 100 mV·$s^{-1}$ until obtaining the characteristic cyclic voltammogram (CV) of a clean Pt surface. The Au electrode was similarly pretreated in 0.5 M $H_2SO_4$ solution in the range from −0.2 to 1.5 V at 100 mV·$s^{-1}$ for 10 min or until the CV characteristic for a clean poly-Au electrode was obtained.

*2.2. Catalyst Preparation.* The electrodeposition of iron was pursued in 0.02 mole·$L^{-1}$ $FeSO_4.7H_2O$ solution by potential cycling technique between −0.855 and −1.205 V at a scan rate of 100 mV·$s^{-1}$ (only two cycles were employed) [32]. The deposited iron was next subjected to an activation at constant potentials (−0.5, −0.9, and −1.3 V) for 10 min in 0.2 mole·$L^{-1}$ NaOH solution. The catalyst was simply abbreviated based on the involved catalytic ingredients. For example, the FeOx/Pt catalyst indicates the electrodeposition of iron onto a poly-Pt electrode where the addition of a prefix "a-" to the catalyst's name outlines the activation process. The letter "x" may vary from 0 (for metallic Fe) to 1.5 (for $Fe_2O_3$).

*2.3. Electrochemical Characterization.* All catalysts were characterized electrochemically before and after modification with FeOx by measuring their characteristic CVs in 0.5 M $H_2SO_4$ (Figure 1), where the corresponding real surface areas of the FeOx/Pt catalysts could be estimated assuming a reference value of 210 $\mu$C·$cm^{-2}$ for $H_{ads/des}$ [33]. The electrocatalytic activity of the prepared catalysts toward FAO was examined in 0.3 M FA (pH = 3.5), where the pH was adjusted using a dilute solution of sodium hydroxide. Electrochemical and impedance measurements were performed at room temperature (25 ± 1°C) in a two-compartment three-electrode Pyrex glass cell (home-made) using an EG&G potentiostat (model 273) operated with E-Chem 270 software. Current densities were calculated for the FeOx/Pt catalysts on the basis of the real surface areas of Pt in the catalyst.

*2.4. Materials Characterization.* In the meanwhile, the catalysts were inspected morphologically by field-emission scanning electron microscopy (FE-SEM, Zeiss Ultra 60) at an acceleration voltage of 8 kV and a working distance of 2.8–3.2 mm. The microscope was fitted with an energy-dispersive X-ray spectroscope (EDX) that reported the elemental composition of the catalyst. Structurally, the catalysts were analyzed using a glancing angle ($\theta$ = 5°) X-ray diffractometer (XRD, PANalytical, Empyrean) operated with Cu target ($\lambda$ = 1.54 Å), where 2$\theta$ varied from 20–120° at a scan rate of 29° $s^{-1}$.

## 3. Results and Discussion

*3.1. Electrochemical Characterization.* Figure 1(a) depicts the CVs of the bare Pt and FeOx/Pt catalysts in 0.5 M $H_2SO_4$ in which the bare Pt catalyst (curve A) possessed the characteristic peaks of poly-Pt substrates with the (Pt ⟶ PtO) oxidation extending over a wide range of potentials (from 0.3 to 1.0 V) and its subsequent reduction at ca. 0.5 V. This associated the popular peaks for hydrogen adsorption

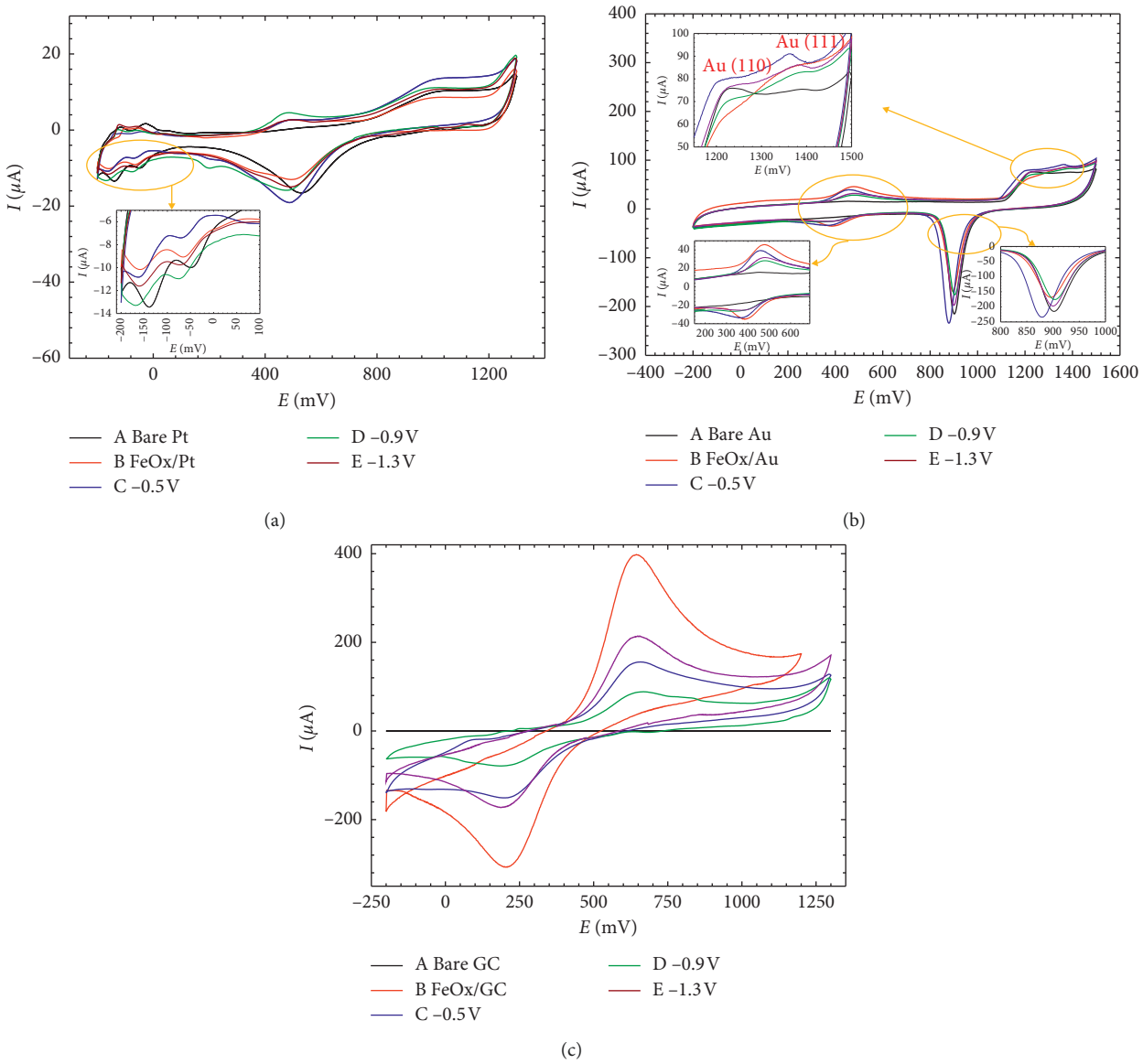


Figure 1: CVs measured in 0.5 M $H_2SO_4$ at a scan rate 100 mV·$s^{-1}$ at bare curve A and nonactivated curve B and activated curve C (at −0.5 V), curve D (at −0.9 V), and curve E (at −1.3 V) nano-FeOx-modified Pt (a), Au (b), and GC (c) substrates. Activation was pursued for 10 min in 0.2 mole·$L^{-1}$ NaOH.

and desorption ($H_{ads}/_{des}$) that appeared between −0.2 and 0.1 V. These peaks appeared split to distinguish the Pt (l00) (A1: at a lower potential) and the Pt (111) (A2: at a higher potential) crystal facets of the bare poly-Pt substrate. The same electrochemical features of Pt retained in the whole investigated the set of FeOx/Pt catalysts (before and after activation—curves B–E of Figure 1(a)). This, interestingly, reflected the partial coverage of the nano-FeOx on the Pt surface that ensures the surface exposure of Pt to the electrolyte (Pt is the base substrate for FA adsorption). Few more things may also be noticed upon the comparison of curves B–E with curve A in Figure 1(a).

(i) A new redox peak at 0.4–0.6 V appeared in Figure 1(a) (curves B–E) after the deposition of nano-FeOx which confirmed the successful deposition of Fe species [34]. This redox couple may likely be assigned to the $Fe/Fe^{2+}$ transformation [32].

(ii) The intensities of Pt ⟶ PtO, PtO ⟶ Pt, and $H_{ads}$ peaks (curve A) decreased with the nano-FeOx deposition (curve B) which agreed consistently with the shrinkage of the real Pt surface area. Consistently, the overall charge consumed in the $H_{ads}$ (A1 + A2) peaks of the FeOx/Pt catalyst decreased (~21%) but the ratio of charges consumed in the $H_{ads}$ peaks (A1 : A2) at the Pt (100) and Pt (111) facets remained almost unchanged. This implies that nano-FeOx was equally deposited at both facets. Table 1 represents the real Pt surface area calculated from the charge consumed in the $H_{ads}$ at the Pt (100) (A1) and Pt (111) (A2) facets and the

Table 1: The real Pt surface areas calculated based on the ($H_{ads}/_{des}$) peaks (A1 and A2) utilizing a reference value of 210 $\mu C \cdot cm^{-2}$ and based on the PtO ⟶ Pt reduction peak (A) utilizing a reference value of 420 $\mu C \cdot cm^{-2}$.

| Electrode | A1 (100)/$cm^2$ | A2 (111)/$cm^2$ | (A1 + A2)/$cm^2$ | (A1 : A2) | A (PtO reduction)/$cm^2$ |
|---|---|---|---|---|---|
| Bare Pt | 0.032 | 0.020 | 0.052 | 1.60 | 0.064 |
| FeOx/Pt | 0.025 | 0.016 | 0.041 | 1.56 | 0.057 |
| a-FeOx/Pt (−0.5 V) | 0.026 | 0.013 | 0.039 | 2.00 | 0.073 |
| a-FeOx/Pt (−0.9 V) | 0.032 | 0.028 | 0.060 | 1.14 | 0.077 |
| a-FeOx/Pt (−1.3 V) | 0.030 | 0.028 | 0.058 | 1.07 | 0.066 |

PtO ⟶ Pt (A)). We should emphasize here that calculations with the PtO ⟶ Pt (A) reduction peak always overestimate the real surface area of Pt as it sometimes overlaps the reduction peaks of dissolved oxygen and iron oxides.

(iii) The data in Table 1 indicate a strong dependence of the A1 : A2 ratio on the activation voltage of the FeOx/Pt catalyst. For example, the activation at −0.5 V inspired a surface reconstruction enriching the Pt (100) (A1) on the expense of the Pt (111) (A2) facets. It also maintained lowering the total (A1 + A2) real surface area of Pt (calculated from the $H_{ads}$ peaks) which disagreed with the large increase of Pt ⟶ PtO and PtO ⟶ Pt peak currents (note also the large increase of the real surface area (0.073 $cm^2$) calculated from the PtO ⟶ Pt reduction peak). A plausible illustration for this contradiction might support the partial $Fe^{2+}/Fe^{3+}$ transformation with the appearance of a new redox couple (the $Fe^{2+}/Fe^{3}$ oxidation overlapping the Pt ⟶ PtO oxidation and the $Fe^{3}/Fe^{2+}$ reduction overlapping the PtO ⟶ Pt peak). The appearance of a new reduction peak at ~0.2 V suggested the existence of two redox couples for iron species, reinforcing this assumption. The decrease in the real surface area of Pt (depicted from the decrease of A1 + A2) suggested a surface oxidation of $Fe^{2+}$ species followed by migration at Pt sites.

(iv) The other extreme of activation that was carried out at −1.3 V increased the overall real surface area of Pt a little (from ~0.052 to 0.058 $cm^2$) but decreased the A1 : A2 ratio (from ~1.56 to 1.07). It inferred as well a surface reconstruction for the Pt facets but this time on the expense of the Pt (100). No reduction peaks were observed at ~0.2 V, and the intensities of the Pt ⟶ PtO and PtO ⟶ Pt peaks remained almost unchanged if compared to their analogies of the bare Pt substrate. We believe that activation of the FeOx/Pt catalyst at −1.3 V motivated the $Fe^{2+}/Fe$ reductive transformation and inspired a self-activation for the Pt surface, increasing its real surface area.

(v) Activation of the FeOx/Pt catalyst between −0.5 V and −1.3 V resulted in the presence of a mixture of $Fe^{2+}$ and $Fe^{3+}$ species at the electrode surface while boosting the $Fe/Fe^{2+}$ oxidative transformation (see the increase of the peak height of the oxidation peak at ~0.5 V).

We paid attention to the phenomenon of surface reconstruction of Pt facets because it might impact strongly the catalytic efficiency of FAO. Grozovski et al. reported recently that Pt (100) domains of Pt nanoparticles were highly active toward FAO and CO poisoning more than the Pt (111) domains [35]. In addition, the modification of the Pt substrate with FeOx enriches the surface with hydroxyl groups that boost the indirect dehydration pathway of FAO [34].

On the contrary, Figures 1(b) and 1(c) track a similar evolution for the FeOx-modified catalysts (in an acidic medium as in Figure 1(a)) but on Au and GC substrates, respectively. We aimed from this inspection to evaluate the role of the substrate and nano-FeOx on the catalytic efficiency of FAO (see later this impact). Figure 1(b) shows clearly the typical characteristic electrochemical response of polycrystalline Au substrates in acidic media for all catalysts with the surface oxidation at the Au (110) and Au (111) facets of poly-Au substrate at ca. 1.2–1.4 V and the subsequent reduction at ca. 0.9 V [36, 37]. The deposition of nano-FeOx resulted in the appearance of a new redox couple at ca. 0.47 V (anodic peak) and 0.39 V (cathodic peak) whose peak intensity depended on the activation potential [38]. The upper inset of Figure 1(b) that magnifies the surface oxidation of poly-Au substrate indicates the preferential deposition of nano-FeOx on the Au (110) with a major reconstruction prevailing the Au (111) orientation. The subsequent activation (all cases) retained mostly the domination of the Au (111) orientation. The intensity of the reduction peak at 0.9 V decreased with the nano-FeOx deposition which inferred its successful deposition. The activation at −0.5 V was odd (if compared to other activation voltages) where all of its faradaic processes appeared enhanced. For the FeOx/GC catalyst, a redox couple for Fe species was obvious at ca. 0.64 V (anodic peak) and 0.21 V (cathodic peak) whose peak intensities decreased upon activation (Figure 1(c)). The activation at −0.5 V resulted in the appearance of a second anodic peak at ~80 mV that probably recommends the existence of iron in two different oxidation states. We were curious, therefore, to inspect the impact of activating the catalyst at −0.5 V morphologically and compositionally.

*3.2. Material Characterization.* Morphologically, the FeOx/Pt catalyst was inspected before and after activation at −0.5 V (Figure 2). It seems nano-FeOx was deposited mostly agglomerated in a sponge-like structure with few nanowires (ca. 20 nm in average diameter and 77 nm in average length, respectively). However, the agglomeration was not homogeneous along the entire Pt surface. Interestingly, upon activation, the agglomeration decreased and many nanowires appeared individually spanning the entire Pt surface.

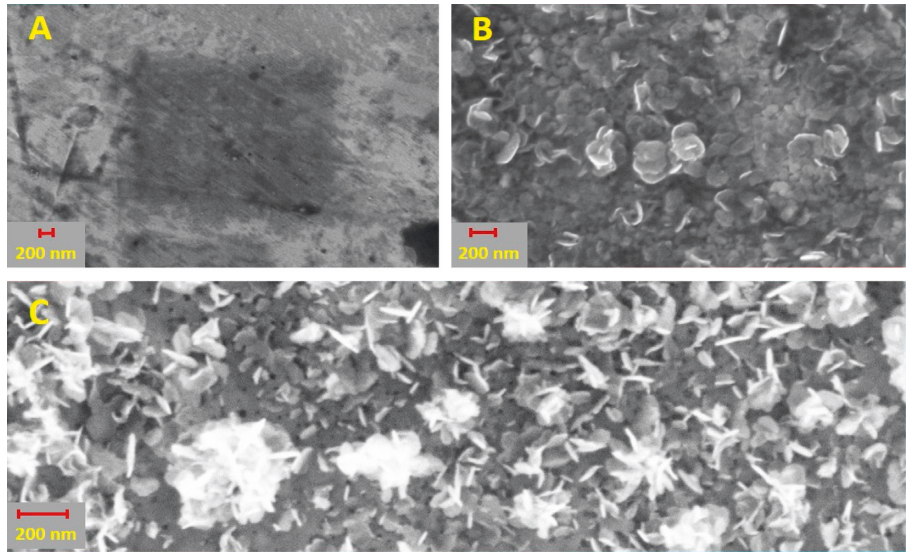


Figure 2: FE-SEM images of the bare Pt (A), FeOx/Pt (B), and a-FeOx/Pt (−0.5 V) (C) catalysts.

The EDX analyses of the three catalysts (Pt, FeOx/Pt and a-FeOx/Pt) in Figure 3 confirms the successful deposition of all relevant components of the catalysts and estimates their relative proportions [39]. One may easily notice, with activation, the relative increase of the oxygen and Pt contents that accompanied a corresponding decrease of the Fe content. Recalling the discrepancy of the surface area measurements utilizing the $H_{ads}$ and PtO ⟶ Pt peaks in Figure 1(a) (see also Table 1) which dealt principally with surface measurements may open a plausible vision for the activation. Evoking that EDX is a bulk analysis (monitoring the composition along a depth in microns), we expect that activation at −0.5 V boosted the surface ($Fe^{2+}/Fe^{3+}$) oxidation and the inward oxygen diffusion along the Pt surface. Meanwhile, it inducted a partial dissolution of iron specious that in solution may get re-adsorbed to subject $Fe^{3+}$ for a reduction in the cathodic-going scan (Figure 1(a)) within the same potential domain of PtO reduction. This, with activation at −0.5 V, increases the charge consumed in the reduction peak at 0.6 V while maintaining almost the same surface area of Pt (a minor change was noticed from the $H_{ads}$ measurements).

The XRD analysis (Figure 4) failed to detect nano-FeOx rather to assign its crystal structure perhaps because of the low detection limit of the instrument or to the existence of nano-FeOx in a minute amount at the surface. Even, glancing the incident radiation at a small angle did not help. However, important information could be revealed by comparing the different diffraction peaks of bare Pt substrate. Basically, the Pt spectra reflected the diffractions at $2\theta$ of 39.8, 46.3, 67.5, and 81.3° of the Pt (111), (200), (220), and (311) planes, respectively, but with different ratios (PDF card: 00-004-0802) [40]. It seems that nano-FeOx was preferentially deposited onto the Pt (111) plane and activation at −0.5 V inspired a surface reconstruction prevailing the Pt (200) diffraction plane.

*3.3. Electrocatalysis of FAO.* The catalytic performance of catalysts was investigated by measuring the CVs of FAO in an aqueous solution of 0.3 M FA (pH 3.5) (Figure 5). Interestingly, the bare Pt electrode (Figure 5(a)) represented the expected behavior of Pt substrates in FA solution where FAO proceeded in two parallel pathways. The first was the direct (desirable) pathway involving the dehydrogenation of FA to $CO_2$ at ca. 0.26 V with a peak current density of $I_p^d$. The other was the indirect (undesirable) pathway involving the chemical dehydration of FA to poisonous CO that could be oxidized at ca. 0.65 V (with a peak current density $I_p^{ind}$)) after getting the Pt surface hydroxylated (Pt–OH) at ca. 0.5 V. Unfortunately, the adsorption of CO on the bare Pt surface in the low potential domain inducts a critical poisoning for the Pt catalyst deactivating most of its active sites and consuming a higher overpotential in undesirable oxidation route. In the backward cathodic-going scan, most of the poisonous CO intermediate has been released to expose a clean Pt surface for FAO through the dehydrogenation pathway. Therefore, the current intensity in the backward scan ($I_b$) increases largely. The level of poisoning or, in other words, the catalytic activity of the catalyst can be evaluated from the relative $I_p^d/I_p^{ind}$ and $I_p^d/I_b$ ratios. A high value of $I_p^d/I_p^{ind}$ indicates a preference of the FAO to proceed via the less energetic (favorable) dehydrogenation pathway. On the contrary, a high value of $I_p^d/I_b$ (hint: the ideal value of $I_p^d/I_b$ =1 for a Pd substrate) infers a high catalytic tolerance of the catalyst toward poisoning with CO. The values of $I_p^d/I_p^{ind}$ and $I_p^d/I_b$ of the bare Pt catalyst were 2.3 and 0.31, respectively. Interestingly, these values changed at the FeOx/Pt catalyst to 9.1 and 0.58, respectively, with a negative shift (ca. −30 mV) in the onset potential of FAO (Table 2). This highlighted the potential role of nano-FeOx in boosting the catalytic performance of the Pt catalyst. In fact, the $I_p^d/I_b$ varied in a narrow domain for the whole set of investigated catalysts. However, the activation of the FeOx/Pt catalyst influenced the activity of the catalyst toward FAO depending on the activation potential. Basically, employing the activation at −0.5 V yielded the best catalytic performance in terms of the $I_p^d/I_p^{ind}$ (17.4, i.e., ~ eightfold enhancement) ratio

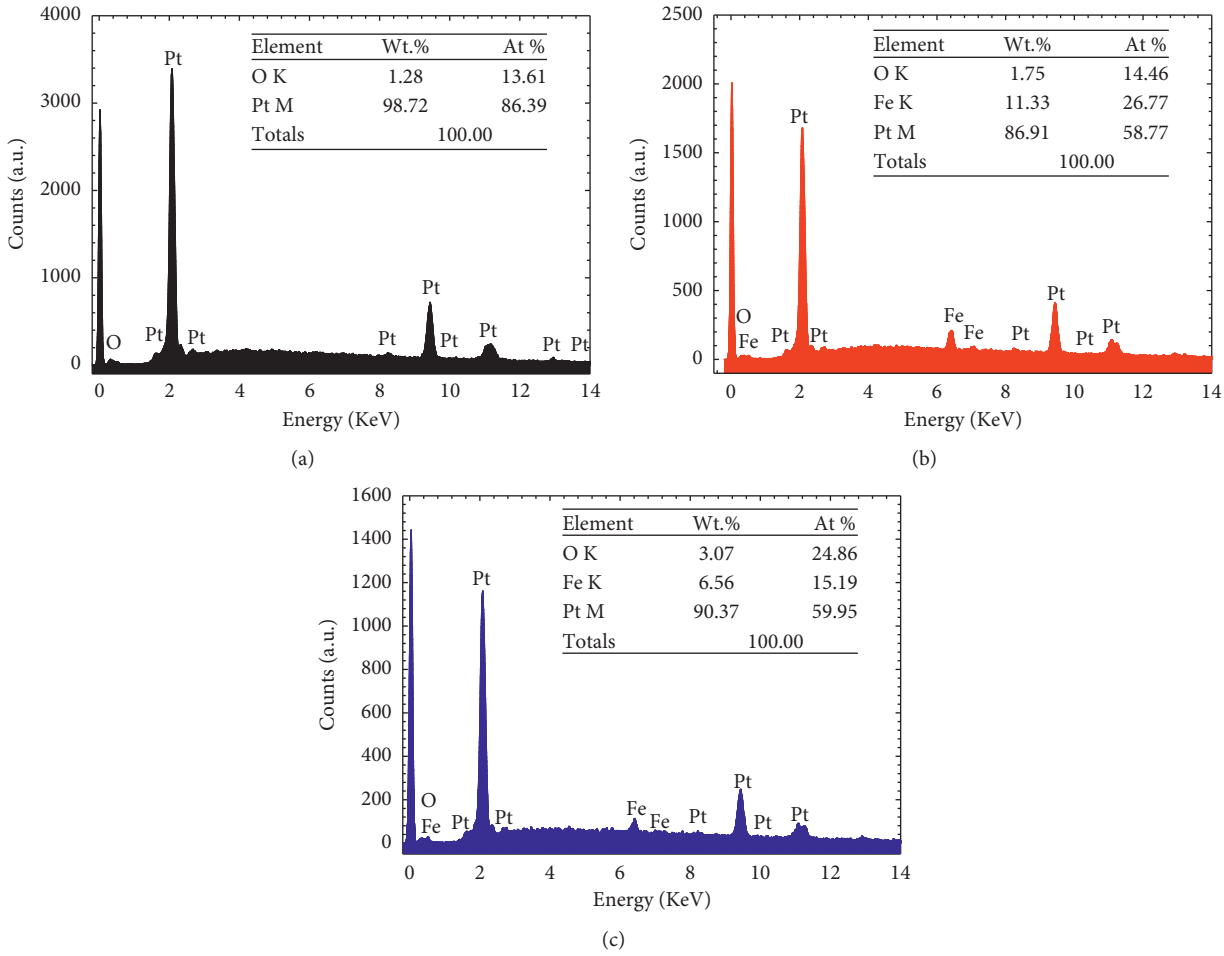


Figure 3: EDX analyses of the bare Pt (a), FeOx/Pt (b), and a-FeOx/Pt (−0.5 V) (c) catalysts.

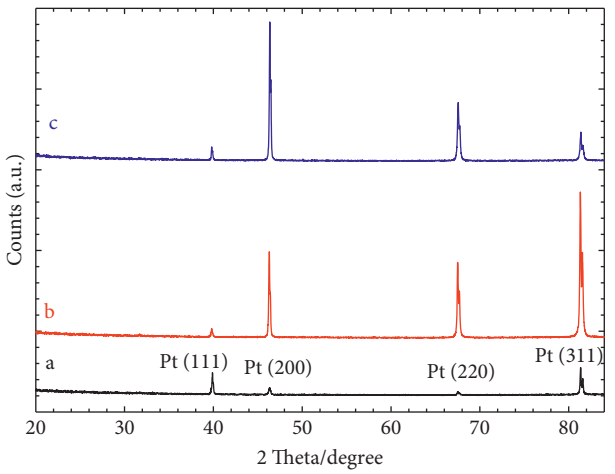


Figure 4: XRD spectra of the bare Pt (a), FeOx/Pt (b), and a-FeOx/Pt (−0.5 V) (c) catalysts.

and the highest negative shift (ca. −30 mV) in the onset potential of FAO (Table 2). Pursuing the activation at −1.3 V came in the second place (after −0.5 V) with an $I_p^d/I_p^{ind}$ ratio of 10.6 (i.e., fivefold enhancement) and a negative shift (ca. −13 mV) in the onset potential of FAO. Activating the FeOx/Pt catalyst in between (−1.3 V to −0.5 V) resulted in less catalytic activity (in terms of $I_p^d/I_p^{ind}$) (Table 2).

On the contrary, the FeOx/Au (Figure 5(b)) and FeOx/GC (Figure 5(c)) catalysts either before or after activation exhibited no catalytic activity toward FAO with the experimental conditions of this investigation. The redox peak couple observed at ca. 0.4 V corresponds to the transformation of Fe species which again confirmed the inertness of not only the bare Au and GC substrates but also the nano-FeOx toward FAO.

*3.4. Stability of the Binary Catalyst.* The stability of catalysts always concerns the industrial fuel cell manufacturer exactly the same as the catalysts' efficiencies. This is, definitely, a commercial view estimating the life-time of the real FCs. In this investigation, the modification of the Pt/GC electrode with nano-FeOx was intended to improve not only the catalytic activity but also the catalytic stability of the catalyst. The stability of the FeOx/Pt catalyst was evaluated by chronoamperometry measurements (Figure 6) at a potential of 0.2 V in a continuous electrolysis experiment which lasted for 3 h. The observed decay in the current density was normal for Pt-based catalysts which resulted either from a surface Pt reconstruction accumulating more poisoning CO

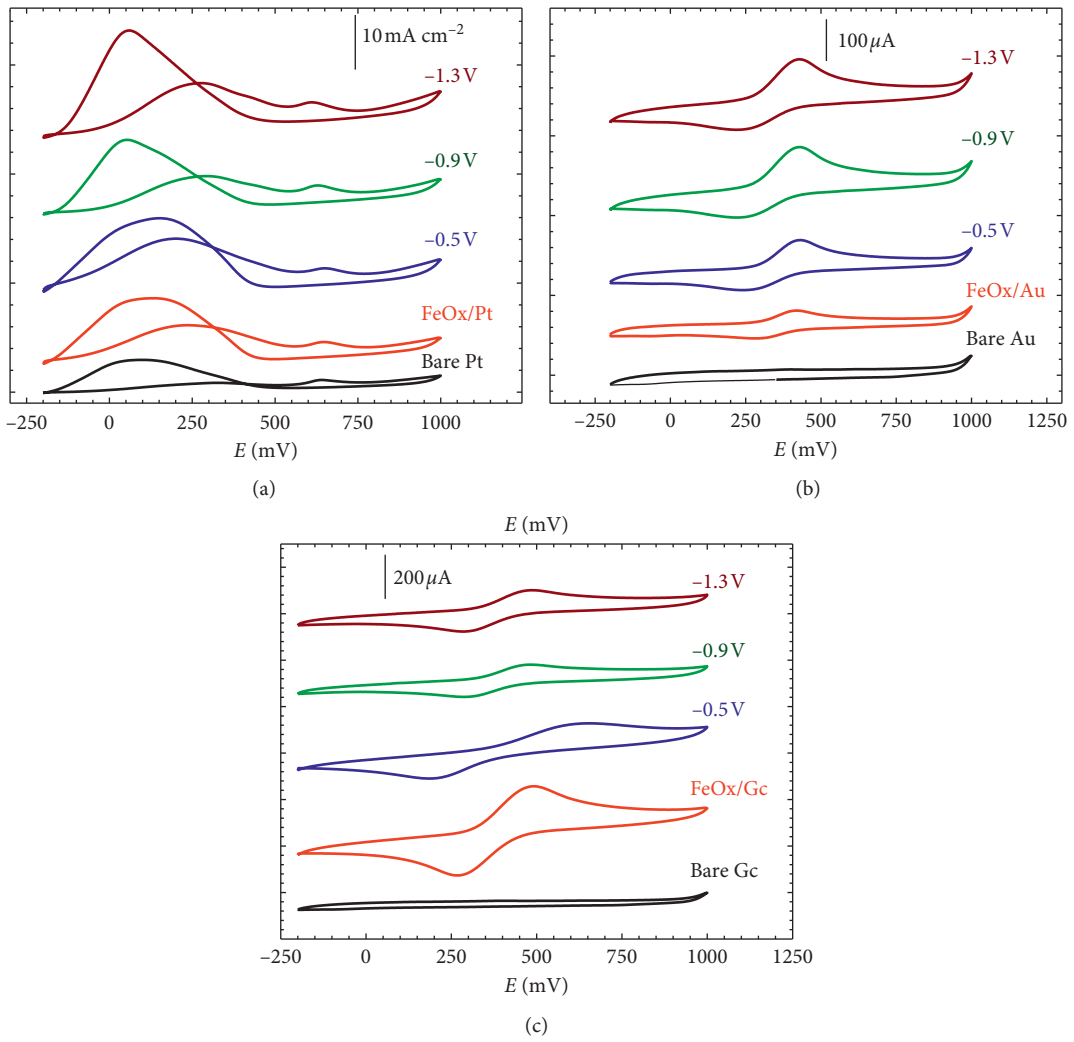


Figure 5: CVs in 0.3 M FA (pH = 3.5) for the bare Pt (a), Au (b), and GC (c) catalysts before and after the modification with nano-FeOx and before and after activation at −0.5, −0.9, and −1.3 V.

Table 2: Electrochemical measurements obtained for FAO.

| Electrodes | $I_d$ (mA cm$^{-2}$) | $I_{ind}$ (mA cm$^{-2}$) | $I_b$ (mA cm$^{-2}$) | $I_d/I_{ind}$ | $I_d/I_b$ | $E_{onset}$ (mV) | $R_{ct}$ (kΩ) |
|---|---|---|---|---|---|---|---|
| Bare Pt | 1.6 | 0.7 | 5.1 | 2.3 | 0.31 | −140 | 82 |
| FeOx/Pt | 6.4 | 0.7 | 11.1 | 9.1 | 0.58 | −170 | 80 |
| a-FeOx/Pt (−0.5 V) | 8.7 | 0.5 | 12.6 | 17.4 | 0.7 | −170 | 64 |
| a-FeOx/Pt (−0.9 V) | 6.6 | 1 | 11.8 | 6.6 | 0.56 | −166 | — |
| a-FeOx/Pt (−1.3 V) | 9.5 | 0.9 | 16.5 | 10.6 | 0.58 | −153 | — |

intermediate or from a mechanical detachment of surface modifiers (as nano-FeOx) that inspired the catalytic enhancement at the beginning. Fortunately, even with the decay, the a-FeOx/Pt exhibited the highest activity and stability after 3 h of continuous electrolysis.

*3.5. Origin of Enhancement.* The electrochemical impedance spectroscopy (EIS) is an effective and attractive technique comparing the internal charge transfer resistance ($R_{ct}$) of a given process in different catalysts [29, 30]. Figure 7 shows the Nyquist plots of the investigated catalyst at open circuit potentials in 0.3 M FA (pH = 3.5) in the frequency range from 10 mHz to 100 kHz. It was obvious that just the deposition of nano-FeOx on the Pt surface was not so effective in lowering $R_{ct}$. However, with the activation of the catalyst (a-FeOx/Pt) at −0.5 V, a large decrease in the semicircle diameter and, hence, $R_{ct}$ was observed (Table 2). This recommended a potential role for the activated nano-FeOx in mediating the reaction mechanism of FAO in the way facilitating the charge transfer. It is believed that the existence of nano-FeOx in several oxidation states was behind the

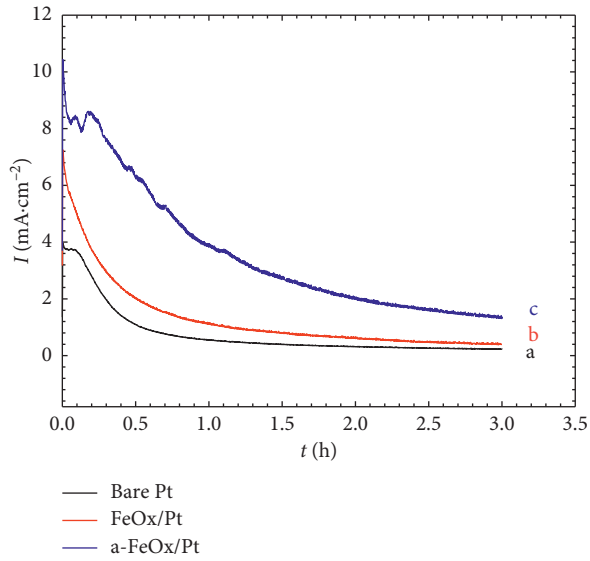


Figure 6: Current transients (I-t) obtained at 0.2 V during FAO at bare Pt (a), FeOx/Pt (b), and a-FeOx/Pt (−0.5 V) (c) electrodes.

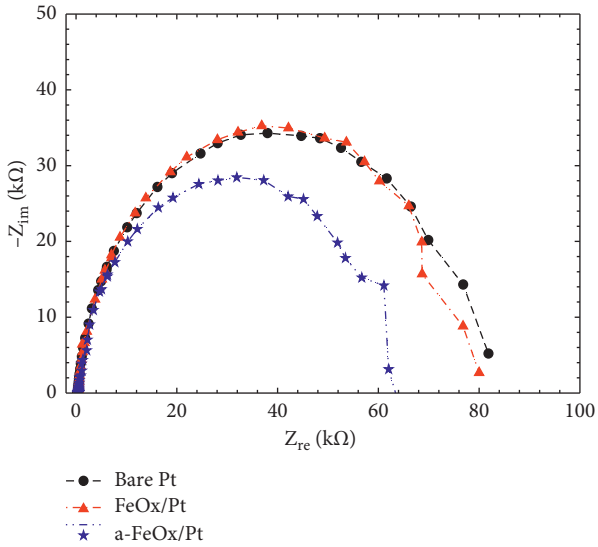


Figure 7: Nyquist plots at open circuit potentials for bare Pt (a), FeOx/Pt (b), and a-FeOx/Pt (−0.5 V) (c) electrodes in 0.3 M FA (pH = 3.5).

boosting inspired electronically. This, perhaps, synergized with the enrichment nano-FeOx stimulated to the Pt surface with oxygen containing species that can definitely enhance the indirect pathway of FAO (bifunctional mechanism).

## 4. Conclusion

A facile synthesis of a binary FeOx/Pt nanoanode for formic acid electro-oxidation (FAO) was presented. The investigation confirmed the substrate's dependence of FAO where a Pt surface was necessary but gold, glassy carbon, and nano-FeOx surfaces showed a complete inertness. The FeOx/Pt catalyst exhibited a better (~4 times) catalytic performance than the bare Pt electrode, and activating the catalyst at −0.5 V boosted the enhancement to ~8 times. The EIS inspection confirmed the electronic role of nano-FeOx in the catalytic enhancement of FAO in the FeOx/Pt catalyst as it succeeded to mediate the reaction with the possible oxidation states it owned in such a way facilitating the charge transfer. The catalyst's activation was conceived to induct a surface reconstruction for the Pt surface sites in such a way enriching the favorable facets for FAO.

## Data Availability

The data used to support the findings of this study are available from the corresponding author upon request.

## Conflicts of Interest

The authors declare that there are no conflicts of interest regarding the publication of this paper.

## Acknowledgments

This research was supported by the General Scientific Research Department at Cairo University (Grant 77/2016).

## References

[1] S. Curtin and J. Gangi, *Fuel Cell Technologies Market Report 2016*, U.S. Department of Energy: Fuel Cell and Hydrogen Energy Association, Washington, DC, USA, 2017.

[2] S. V. M. Guaitolini and J. F. Fardin, "4—fuel cells: history (short remind), principles of operation, main features, and applications A2—yahyaoui, imene," in *Advances in Renewable Energies and Power Technologies*, pp. 123–150, Elsevier, Amsterdam, Netherlands, 2018.

[3] V. Das, S. Padmanaban, K. Venkitusamy, R. Selvamuthukumaran, F. Blaabjerg, and P. Siano, "Recent advances and challenges of fuel cell based power system architectures and control—a review," *Renewable and Sustainable Energy Reviews*, vol. 73, pp. 10–18, 2017.

[4] A. Eftekhari and B. Fang, "Electrochemical hydrogen storage: opportunities for fuel storage, batteries, fuel cells, and supercapacitors," *International Journal of Hydrogen Energy*, vol. 42, no. 40, pp. 25143–25165, 2017.

[5] M. Nacef and A. M. Affoune, "Comparison between direct small molecular weight alcohols fuel cells' and hydrogen fuel cell's parameters at low and high temperature. Thermodynamic study," *International Journal of Hydrogen Energy*, vol. 36, no. 6, pp. 4208–4219, 2011.

[6] L. Chen, J. Zhu, C. Xuan et al., "Effects of crystal phase and composition on structurally ordered Pt-Co-Ni/C ternary intermetallic electrocatalysts for the formic acid oxidation reaction," *Journal of Materials Chemistry A*, vol. 6, no. 14, pp. 5848–5855, 2018.

[7] A. Feng, J. Bai, W. Shao, W. Hong, Z. Q. Tian, and Z. Xiao, "Surfactant-free Pd–Fe nanoparticles supported on reduced graphene oxide as nanocatalyst for formic acid oxidation," *International Journal of Hydrogen Energy*, vol. 42, no. 22, pp. 15196–15202, 2017.

[8] T. Tsujiguchi, F. Matsuoka, Y. Hokari, Y. Osaka, and A. Kodama, "Overpotential analysis of the direct formic acid fuel cell," *Electrochimica Acta*, vol. 197, pp. 32–38, 2016.

[9] I. M. Al-Akraa, A. M. Mohammad, M. S. El-Deab, and B. E. El-Anadouli, "Electrooxidation of formic acid at platinum-gold nanoparticle-modified electrodes," *Chemistry Letters*, vol. 40, no. 12, pp. 1374-1375, 2011.

[10] I. M. Al-Akraa, A. M. Mohammad, M. S. El-Deab, and B. E. El-Anadouli, "Development of tailor-designed gold-platinum nanoparticles binary catalysts for efficient formic acid electrooxidation," *International Journal of Electrochemical Science*, vol. 7, pp. 3939–3946, 2012.

[11] I. M. Al-Akraa, A. M. Mohammad, M. S. El-Deab, and B. E. El-Anadouli, "Electrocatalysis by design: synergistic catalytic enhancement of formic acid electro-oxidation at core-shell Pd/Pt nanocatalysts," *International Journal of Hydrogen Energy*, vol. 40, no. 4, pp. 1789–1794, 2015.

[12] M. S. El-Deab, G. A. El-Nagar, A. M. Mohammad, and B. E. El-Anadouli, "Fuel blends: enhanced electro-oxidation of formic acid in its blend with methanol at platinum nanoparticles modified glassy carbon electrodes," *Journal of Power Sources*, vol. 286, pp. 504–509, 2015.

[13] M. S. El-Deab, A. M. Mohammad, G. A. El-Nagar, and B. E. El-Anadouli, "Impurities contributing to catalysis: enhanced electro-oxidation of formic acid at Pt/GC electrodes in the presence of vinyl acetate," *Journal of Physical Chemistry C*, vol. 118, no. 39, pp. 22457–22464, 2014.

[14] G. A. El-Nagar, A. M. Mohammad, M. S. El-Deab, T. Ohsaka, and B. E. El-Anadouli, "Acrylonitrile-contamination induced enhancement of formic acid electro-oxidation at platinum nanoparticles modified glassy carbon electrodes," *Journal of Power Sources*, vol. 265, pp. 57–61, 2014.

[15] M. S. Çögenli and A. B. Yurtcan, "Catalytic activity, stability and impedance behavior of PtRu/C, PtPd/C and PtSn/C bimetallic catalysts toward methanol and formic acid oxidation," *International Journal of Hydrogen Energy*, vol. 43, no. 23, pp. 10698–10709, 2018.

[16] H. Fan, M. Cheng, L. Wang, Y. Song, Y. Cui, and R. Wang, "Extraordinary electrocatalytic performance for formic acid oxidation by the synergistic effect of Pt and Au on carbon black," *Nano Energy*, vol. 48, pp. 1–9, 2018.

[17] W. L. Qu, Z. B. Wang, Y. Gao et al., "WO3/C supported Pd catalysts for formic acid electro-oxidation activity," *International Journal of Hydrogen Energy*, vol. 43, no. 1, pp. 407–416, 2018.

[18] Q. Zhao, C. Ge, Y. Cai, Q. Qiao, and X. Jia, "Silsesquioxane stabilized platinum-palladium alloy nanoparticles with morphology evolution and enhanced electrocatalytic oxidation of formic acid," *Journal of Colloid and Interface Science*, vol. 514, pp. 425–432, 2018.

[19] N. He, Y. Gong, Y. Yang et al., "An effective Pd@Ni-B/C anode catalyst for electro-oxidation of formic acid," *International Journal of Hydrogen Energy*, vol. 43, no. 6, pp. 3216–3222, 2018.

[20] F. M. Li, Y. Q. Kang, H. M. Liu, Y. N. Zhai, M. C. Hu, and Y. Chen, "Atoms diffusion-induced phase engineering of platinum-gold alloy nanocrystals with high electrocatalytic performance for the formic acid oxidation reaction," *Journal of Colloid and Interface Science*, vol. 514, pp. 299–305, 2018.

[21] H. Yin, K. Zhou, S. F. Yuan, and Z. R. Chen, "Kinetic study on formaldehyde and formic acid oxidation catalyzed by Pt/C," *Journal of Chemical Engineering of Chinese Universities*, vol. 31, pp. 870–876, 2017.

[22] W. Yu, Z. Xin, W. Zhang et al., "The role of surface functionalities in fabricating supported Pd-P nanoparticles for efficient formic acid oxidation," *Chemical Physics Letters*, vol. 686, pp. 155–160, 2017.

[23] F. Zhou, J. Chen, Y. Wang et al., "The study of platinum-tellurium intermetallic nanoparticles for formic acid electro-oxidation," *Electrochimica Acta*, vol. 248, pp. 307–312, 2017.

[24] F. Zhou, J. Chen, Y. Wang et al., "Remarkable catalytic activity of electrochemically dealloyed platinum–tellurium nanoparticles towards formic acid electro-oxidation," *International Journal of Hydrogen Energy*, vol. 42, no. 26, pp. 16489–16494, 2017.

[25] Z. Liu, G. Fu, J. Li et al., "Facile synthesis based on novel carbon-supported cyanogel of structurally ordered Pd3Fe/C as electrocatalyst for formic acid oxidation," *Nano Research*, vol. 11, no. 9, pp. 4686–4696, 2018.

[26] A. Shafaei Douk, H. Saravani, and M. Noroozifar, "A fast method to prepare Pd-Co nanostructures decorated on graphene as excellent electrocatalyst toward formic acid oxidation," *Journal of Alloys and Compounds*, vol. 739, pp. 882–891, 2018.

[27] T. Szumełda, A. Drelinkiewicz, E. Lalik, R. Kosydar, D. Duraczyńska, and J. Gurgul, "Carbon-supported Pd100-XAuX alloy nanoparticles for the electrocatalytic oxidation of formic acid: influence of metal particles composition on activity enhancement," *Applied Catalysis B: Environmental*, vol. 221, pp. 393–405, 2018.

[28] H. Xu, B. Yan, S. Li et al., "N-doped graphene supported PtAu/Pt intermetallic core/dendritic shell nanocrystals for efficient electrocatalytic oxidation of formic acid," *Chemical Engineering Journal*, vol. 334, pp. 2638–2646, 2018.

[29] R. Zhao, Z. Liu, M. Gong et al., "Ethylenediamine tetramethylene phosphonic acid assisted synthesis of palladium nanocubes and their electrocatalysis of formic acid oxidation," *Journal of Solid State Electrochemistry*, vol. 21, no. 5, pp. 1297–1303, 2017.

[30] C. Zhu, D. Liu, Z. Chen, L. Li, and T. You, "Superior catalytic activity of Pt/carbon nanohorns nanocomposites toward methanol and formic acid oxidation reactions," *Journal of Colloid and Interface Science*, vol. 511, pp. 77–83, 2018.

[31] M. S. El-Deab, M. I. Awad, A. M. Mohammad, and T. Ohsaka, "Enhanced water electrolysis: electrocatalytic generation of oxygen gas at manganese oxide nanorods modified electrodes," *Electrochemistry Communications*, vol. 9, no. 8, pp. 2082–2087, 2007.

[32] Y. X. Chen, S. P. Chen, Q. S. Chen, Z. Y. Zhou, and S. G. Sun, "Electrochemical preparation of iron cuboid nanoparticles and their catalytic properties for nitrite reduction," *Electrochimica Acta*, vol. 53, no. 23, pp. 6938–6943, 2008.

[33] G. A. El-Nagar, M. A. Hassan, I. Lauermann, and C. Roth, "Efficient direct formic acid fuel cells (DFAFCs) anode derived from seafood waste: migration mechanism," *Scientific Reports*, vol. 7, no. 1, article 17818, 2017.

[34] J. R. Rodriguez, R. M. Félix, E. A. Reynoso et al., "Synthesis of Pt and Pt-Fe nanoparticles supported on MWCNTs used as electrocatalysts in the methanol oxidation reaction," *Journal of Energy Chemistry*, vol. 23, no. 4, pp. 483–490, 2014.

[35] V. Grozovski, J. Solla-Gullón, V. Climent, E. Herrero, and J. M. Feliu, "Formic acid oxidation on shape-controlled Pt nanoparticles studied by pulsed voltammetry," *The Journal of Physical Chemistry C*, vol. 114, no. 32, pp. 13802–13812, 2010.

[36] C. Jeyabharathi, P. Ahrens, U. Hasse, and F. Scholz, "Identification of low-index crystal planes of polycrystalline gold on the basis of electrochemical oxide layer formation," *Journal of Solid State Electrochemistry*, vol. 20, no. 11, pp. 3025–3031, 2016.

[37] A. M. Mohammad, M. I. Awad, M. S. El-Deab, T. Okajima, and T. Ohsaka, "Electrocatalysis by nanoparticles: optimization of

the loading level and operating pH for the oxygen evolution at crystallographically oriented manganese oxide nanorods modified electrodes," *Electrochimica Acta*, vol. 53, no. 13, pp. 4351–4358, 2008.

[38] L. Yi, W. Wei, C. Zhao, L. Tian, J. Liu, and X. Wang, "Enhanced activity of Au–Fe/C anodic electrocatalyst for direct borohydride-hydrogen peroxide fuel cell," *Journal of Power Sources*, vol. 285, pp. 325–333, 2015.

[39] S. Shamsuddin, S. B. Jamaludin, Z. Hussain, and Z. A. Ahmad, "Characterization of Fe-Cr-Al2O3 composites fabricated by powder metallurgy method with varying weight percentage of alumina," *Journal of Physical Science*, vol. 19, no. 1, pp. 89–95, 2008.

[40] A. C. Garcia, E. B. Ferreira, V. V. Silva de Barros, J. J. Linares, and G. Tremiliosi-Filho, "PtAg/MnOx/C as a promising electrocatalyst for glycerol electro-oxidation in alkaline medium," *Journal of Electroanalytical Chemistry*, vol. 793, pp. 188–196, 2017.